# A level set method for fluid-structure interactions with immersed surfaces

Georges-Henri Cottet

*LMC-IMAG, Université Joseph Fourier, BP 53, 38041 Grenoble Cedex 9, France*
*Georges-Henri.Cottet@imag.fr*

Emmanuel Maitre

*LMC-IMAG, Université Joseph Fourier, BP 53, 38041 Grenoble Cedex 9, France*
*Emmanuel.Maitre@imag.fr*

Received (Day Month Year)
Revised (Day Month Year)
Communicated by (xxxxxxxxxx)

This paper is devoted to the derivation and the validation of a level set method for fluid-structure interaction problems with immersed surfaces. The test case of a pressurized membrane is used to compare our method to Peskin's Immersed Boundary methods in the two-dimensional case and to demonstrate its capabilities for three-dimensional flows. The method in particular exhibits appealing mass and energy conservation properties.

*Keywords*: Fluid-structure; immersed boundary method; level set.

AMS Subject Classification: 74F10, 76D05, 65M06

## 1. Introduction

Numerical simulations of fluid-structure interactions are among the most challenging problems in computational mechanics. One reason is that the solution of these problems must couple, through interface conditions, different types of models: Eulerian for the flow and Lagrangian for the solid. The most classical approach is the so-called Arbitrary Lagrangian Eulerian (ALE) method [4,18]. In this method the flow part of the problem is solved in a Lagrangian fashion on a mesh that follows the normal displacement of the interface. These methods are in general based on linearization of the flow solver which may affect the accuracy of the results. Moreover large deformations, to say nothing of topology changes, can be difficult to track with ALE methods.

An important particular case of fluid-structure interactions is when structures are low-dimensional sets immersed in the fluid. In that case, the structure dynamics and fluid-structure interface conditions are replaced by a singular forcing term in the flow equations, which dramatically simplifies the coupling. The method of immersed boundaries has been proposed by Peskin [14] to address this type of problems. In this approach immersed one dimensional fibers are discretized by Lagrangian trackers. The elastic force resulting from the stretching of the fibers is estimated from the location of these markers at every time-step. This method has been succesfully applied in a number of situations (see [15] for a review and references therein). This method has however some drawbacks related to the way the force is spread to grid points. This is generally acknowledged to be responsible for possible leaking of the method. Although some important recent developments have been made to correct this problem [11,16], this is at the expense of giving up the inherent simplicity of the method. The need to insert or delete markers in case of large deformations is another delicate aspect of the method which requires precise tuning of additional parameters.

Both ALE and immersed boundary methods belong to the class of front tracking methods. Front capturing methods are another class where one tries to follow the interface in an implicit way. The level set method we describe here is in this spirit. Level set methods are now a classical framework to capture Lagrangian interfaces [1,13]. Geometric information on the interface, such as the curvature, can be recovered from the level set function. A level set formulation of immersed boundary problems was announced previously[3]. This paper is devoted to detailed proofs of the results announced in [3], and numerical validation of the method.

This method stems from the observation that in incompressible flows the level set function also carries information on the stretching of the interface. This enables us to rephrase elastic energy and forces in terms of the level set function and a smoothing function. Fluid-structure problems are then entirely described by the Navier-Stokes equations, supplemented by a scalar advection equation for the level set function. To avoid redistancing techniques which are in general used to maintain the interface width at a constant value, and which in our case would have to be taken into account to track the stretching of the interface, we use a renormalization of the smoothing function.

The main features of the method are its simplicity, including for the case of variable density, variable viscosity three-dimensional flows, and its natural control of mass and energy. As a matter of fact, we are able to prove an energy equation which ensures in particular that the regularization of the force does not involve any energy dissipation.

The paper is structured as follows: in section 2 we derive the level set method from energy principles and prove energy estimates. In section 3 we give some details on our numerical implementations of the fluid and transport equations and of the interface forces using renormalized smoothing. In section 4 we present some numerical validations of the method. Finally section 5 is devoted to concluding remarks and discussion of ongoing applications and extensions of the method.

## 2. Level set formulation

The fluid-structure interaction problem we consider consists of an immersed elastic surface in a three dimensional incompressible flow. In that system, the action-reaction principle requires that the jump in the stresses in the flow balances the elastic forces imparted by the immersed interface. Equivalently, elastic forces appear as a singular forcing term in the Navier-Stokes equations written throughout the fluid-structure computational domain.

Following Peskin, [14] we derive this elastic force from an energy functional localized on the interface $\Gamma$:

$$\mathcal{E} = \int_\Gamma E(T) d\sigma \tag{2.1}$$

where $T$ denotes the surface stretching. In the rest of this section we give a level set formulation of this model. We proceed as follows: we first express the interface stretching in terms of a level set function. We then derive a regularized energy functional in terms of the level set function and a cut-off function. We finally deduce an expression for the elastic force and write the complete Navier-Stokes system. We prove for this system an energy principle which guarantees the consistency of the model with the original fluid-structure problem.

In contrast with [3] where our arguments used parametric representations of the interface, our proofs here are more geometric in the sense that they use intrinsic surface representations. For the sake of simplicity, we have chosen to assume in the sequel periodic boundary conditions (see also the remark below at the end of section 2.5).

### 2.1. *Surface stretching and level set function*

We consider an elastic hyper-surface $\Gamma_t$ immersed in an incompressible fluid governed by the Navier-Stokes equations. This hypersurface, that we call thereafter the membrane, is described at time $t$ by the zero level

set of a function $\phi(\cdot,t):\mathbb{R}^n\to\mathbb{R}$, which is given as $\phi_0$ for $t=0$ and to be determined for $t>0$. While moving with the fluid velocity $\mathbf{u}$, this level set function classically satisfies a transport equation:

$$\phi_t+\mathbf{u}\cdot\boldsymbol{\nabla}\phi=0. \tag{2.2}$$

The normal to the interface is given by $\frac{\boldsymbol{\nabla}\phi}{|\boldsymbol{\nabla}\phi|}$ and its (mean) curvature is $\kappa(\phi)=\boldsymbol{\nabla}\cdot\frac{\boldsymbol{\nabla}\phi}{|\boldsymbol{\nabla}\phi|}$. One key point of our method is to remark that as the flow is incompressible, the function $\phi$ not only represents the geometry of the membrane, but also carries some information on its stretching (more precisely on the variation of surface area). To show this, we first need the following technical lemma:

**Lemma 2.1.** *Let $\phi:\mathbb{R}^n\to\mathbb{R}$ be Lipschitz over $\mathbb{R}^n$ and such that $|\boldsymbol{\nabla}\phi|$ is bounded from below by some positive constant. Let $g\in L^1(\mathbb{R}^n)$, then, for $\eta>0$ sufficiently small,*

$$\int_{|\phi(x)|<\eta} g(\mathbf{x})d\mathbf{x}=\int_{-\eta}^{\eta}\int_{\{\phi(\mathbf{x})=\nu\}} g(\mathbf{x})|\boldsymbol{\nabla}\phi|^{-1}d\boldsymbol{\sigma}d\nu.$$

**Proof.** This is a straightforward consequence of [5], proposition 3, page 118. A more intuitive proof is to write a volume element $d\mathbf{x}$ in a neighborhood of $\mathbf{x}$ as $d\mathbf{x}=d\boldsymbol{\sigma}\times dh$, where $d\boldsymbol{\sigma}$ is the surface measure of $\phi(\mathbf{x})=\nu$ and $dh$ is along the normal vector $\frac{\boldsymbol{\nabla}\phi}{|\boldsymbol{\nabla}\phi|}$. Then the expansion

$$\nu\pm d\nu:=\phi(\mathbf{x}\pm dh\frac{\boldsymbol{\nabla}\phi}{|\boldsymbol{\nabla}\phi|})=\phi(\mathbf{x})\pm dh|\nabla\phi|+O(dh^2)$$

yields $d\mathbf{x}=|\boldsymbol{\nabla}\phi|^{-1}d\boldsymbol{\sigma}d\nu$. □

Let us denote by $\mathbf{X}(s;\mathbf{x},t)$ the characteristic curves, i.e. the solution of the differential system $\frac{d\mathbf{X}}{ds}=\mathbf{u}(\mathbf{X}(s),s)$ with initial condition $\mathbf{x}$ at $s=t$. Let $\Omega$ an open bounded subset of $\mathbb{R}^n$. We assume the following regularity on the initial curve and the velocity field:

$$(A)\qquad \phi_0\in\mathcal{C}^2(\overline{\Omega}),\quad |\nabla\phi_0|\geq\alpha>0,\quad \mathbf{u}\in\mathcal{C}^2(\overline{\Omega}\times[0,T]),\quad \boldsymbol{\nabla}\cdot\mathbf{u}=0$$

**Proposition 2.1.** *Under assumption $(A)$, let $\phi$ be the $\mathcal{C}^2$ solution of (2.2) with initial condition $\phi(0)=\phi_0$. Then for every $f\in\mathcal{C}_c(\Omega)$,*

$$\int_{\{\phi_0(\boldsymbol{\xi})=0\}} f(\boldsymbol{\xi})|\boldsymbol{\nabla}\phi_0(\boldsymbol{\xi})|^{-1}d\sigma(\boldsymbol{\xi})=\int_{\{\phi(\mathbf{x},t)=0\}} f(\mathbf{X}(0;\mathbf{x},t))|\boldsymbol{\nabla}\phi(\mathbf{x},t)|^{-1}d\boldsymbol{\sigma}(\mathbf{x}).$$

**Proof.** As will be proved in the appendix, assumption $(A)$ implies that

$$s\to\int_{\{\phi_0=s\}} f(\boldsymbol{\xi})|\boldsymbol{\nabla}\phi_0(\boldsymbol{\xi})|^{-1}d\boldsymbol{\sigma}(\boldsymbol{\xi})$$

is continuous. Thus using Lemma 2.1,

$$\begin{aligned}\int_{\{\phi_0(\boldsymbol{\xi})=0\}} f(\boldsymbol{\xi})|\boldsymbol{\nabla}\phi_0(\boldsymbol{\xi})|^{-1}d\sigma(\boldsymbol{\xi})&=\lim_{\eta\to0}\frac{1}{\eta}\int_{-\frac{\eta}{2}}^{\frac{\eta}{2}}\int_{\{\phi_0(\boldsymbol{\xi})=\nu\}} f(\boldsymbol{\xi})|\boldsymbol{\nabla}\phi_0(\boldsymbol{\xi})|^{-1}d\sigma(\boldsymbol{\xi})d\nu\\&=\lim_{\eta\to0}\frac{1}{\eta}\int_{\{|\phi_0(\boldsymbol{\xi})|<\frac{\eta}{2}\}} f(\boldsymbol{\xi})d\xi\end{aligned}$$

We perform the change of variable $\boldsymbol{\xi}=\mathbf{X}(0;\mathbf{x},t)$ whose Jacobian $J(0;\mathbf{x},t)$ is equal to 1 since $\boldsymbol{\nabla}\cdot\mathbf{u}=0$. As $\phi$ is a solution of a transport equation one has $\phi_0(\mathbf{X}(0;\mathbf{x},t))=\phi(\mathbf{x},t)$. Therefore

$$\int_{\{\phi_0(\boldsymbol{\xi})=0\}} f(\boldsymbol{\xi})|\boldsymbol{\nabla}\phi_0(\boldsymbol{\xi})|^{-1}d\sigma(\boldsymbol{\xi})=\lim_{\eta\to0}\frac{1}{\eta}\int_{\{|\phi(\mathbf{x},t)|<\frac{\eta}{2}\}} f(\mathbf{X}(0;\mathbf{x},t))d\mathbf{x}$$

which thanks to Lemma 2.1 leads to the expected result. □

### 2.2. *Link with Lagrangian formulation*

The meaning of this last result is that $|\nabla\phi|/|\nabla\phi_0|$ accounts for the variation of surface measure of $\Gamma_t$ with respect to $\Gamma_0$, and thus yields the elastic force imparted by the immersed surface. To be more explicit, let us make the link between this Eulerian description and the classical Lagrangian point of view (used for example in [11,12,19]). Writing the length measure in terms of a parametrization $\boldsymbol{\gamma}$ and using $\mathbf{X}(0;\boldsymbol{\gamma}(s,t),t) = \boldsymbol{\gamma}(s,0)$ it is not difficult to deduce from Proposition 2.1

**Corollary 2.1.** *With the same assumptions and notation as in Proposition 2.1:*
*i) In two dimensions, let $s \in [0,L] \mapsto \boldsymbol{\gamma}(s,t) \in \mathbb{R}^2$ be a parametrization of $\Gamma_t$. Then one has*

$$\int_0^L f(\boldsymbol{\gamma}(s,0))|\nabla\phi_0(\boldsymbol{\gamma}(s,0))|^{-1}|\boldsymbol{\gamma}_s(s,0)|ds = \int_0^L f(\boldsymbol{\gamma}(s,0))|\nabla\phi(\boldsymbol{\gamma}(s,t),t)|^{-1}|\boldsymbol{\gamma}_s(s,t)|ds$$

*and thus*

$$\frac{|\nabla\phi(\boldsymbol{\gamma}(s,t),t)|}{|\nabla\phi_0(\boldsymbol{\gamma}(s,0))|} = \frac{|\boldsymbol{\gamma}_s(s,t)|}{|\boldsymbol{\gamma}_s(s,0)|}$$

*ii) In three dimensions if $\mathbf{s} = (s_1,s_2) \in \omega \mapsto \boldsymbol{\gamma}(s_1,s_2,t) \in \mathbb{R}^3$ is a (patch of) parametrization of $\Gamma$, one has*

$$\int_\omega f(\boldsymbol{\gamma}(\mathbf{s},0))|\nabla\phi_0(\boldsymbol{\gamma}(\mathbf{s},0))|^{-1}|\boldsymbol{\gamma}_{s_1}(\mathbf{s},0)\times\boldsymbol{\gamma}_{s_2}(\mathbf{s},0)|\,d\mathbf{s}$$
$$= \int_\omega f(\boldsymbol{\gamma}(\mathbf{s},0))|\nabla\phi(\boldsymbol{\gamma}(\mathbf{s},t),t)|^{-1}|\boldsymbol{\gamma}_{s_1}(\mathbf{s},t)\times\boldsymbol{\gamma}_{s_2}(\mathbf{s},t)|d\mathbf{s}$$

*and thus*

$$\frac{|\nabla\phi(\boldsymbol{\gamma}(\mathbf{s},t),t)|}{|\nabla\phi_0(\boldsymbol{\gamma}(\mathbf{s},0))|} = \frac{|\boldsymbol{\gamma}_{s_1}(\mathbf{s},t)\times\boldsymbol{\gamma}_{s_2}(\mathbf{s},t)|}{|\boldsymbol{\gamma}_{s_1}(\mathbf{s},0)\times\boldsymbol{\gamma}_{s_2}(\mathbf{s},0)|}$$

Practically speaking, in the dimension two case, one constructs $\phi_0$ such that its zero level set is $\Gamma_0$, and such that

$$|\nabla\phi_0(\boldsymbol{\gamma}(s,0))| = \frac{|\boldsymbol{\gamma}_s(s,0)|}{|\boldsymbol{\theta}_s(s)|}$$

where $|\boldsymbol{\theta}|$ is a parametrization of the material curve at rest (which can be taken as $\boldsymbol{\gamma}(\cdot,0)$ if the curve is initially unstreched). Then one has for all time $t$

$$|\nabla\phi(\boldsymbol{\gamma}(s,t),t)| = \frac{|\boldsymbol{\gamma}_s(s,t)|}{|\boldsymbol{\theta}_s(s)|}$$

Moreover, if the initial stretching does not depend on $s$ then one can initialize $\phi_0$ as this stretching times the signed distance to the membrane. A similar construction can be used in the 3D case.

### 2.3. *Spreading of interface*

As usual in immersed boundary methods, the elastic force which is concentrated on the membrane has to be spread to a volume force with support in a neighborhood of the interface. In our Eulerian approach, we thus have to express this volume approximation of a Dirac mass $\delta$ with support on the interface, using the function $\phi$ and a regularization function $\zeta$. Let $\mathcal{M}(\Omega)$ be the dual of the space $\mathcal{C}_c(\Omega)$ of continuous functions with compact support endowed with its usual weak convergence.

**Proposition 2.2.** *Let $r \to \zeta(r)$ be a $\mathcal{C}^\infty$ function with support within $[-1,1]$, such that $r \to \frac{1}{\varepsilon}\zeta(\frac{r}{\varepsilon})$ converges when $\varepsilon \to 0$ to $\delta_0$ in $\mathcal{D}'(\mathbb{R})$. Then under assumption $(A)$, when $\varepsilon \to 0$,*

$$\frac{1}{\varepsilon}\zeta\left(\frac{\phi}{\varepsilon}\right)|\nabla\phi| \rightharpoonup \delta_{\{\phi=0\}} \quad \textit{in } \mathcal{M}(\Omega)$$

**Proof.** This result is reminiscent of the work of [1], but for the sake of completeness we give here a more direct proof. For a continuous function $r \to g(r)$, one has by assumption $\int_{\mathbb{R}} \frac{1}{\varepsilon}\zeta\left(\frac{r}{\varepsilon}\right) g(r)\,dr \to g(0)$. Let $f \in \mathcal{C}_c(\Omega)$. From $(A)$ and the appendix, the function $g$ defined by

$$g(r) = \int_{\{\phi=r\}} f\,d\boldsymbol{\sigma}$$

is continuous and we have

$$\int_{\mathbb{R}} \frac{1}{\varepsilon}\zeta\left(\frac{r}{\varepsilon}\right) \int_{\{\phi=r\}} f\,d\boldsymbol{\sigma}\,dr = \int_{\mathbb{R}}\int_{\{\phi=r\}} \frac{1}{\varepsilon}\zeta\left(\frac{\phi}{\varepsilon}\right) f\,d\boldsymbol{\sigma}\,dr \to \int_{\{\phi=0\}} f\,d\boldsymbol{\sigma}.$$

Using the support of $\zeta$, and Lemma 2.1,

$$\begin{aligned}\int_{\mathbb{R}}\int_{\{\phi=r\}} \frac{1}{\varepsilon}\zeta\left(\frac{\phi}{\varepsilon}\right) f\,d\boldsymbol{\sigma}\,dr = \int_{-\varepsilon}^{\varepsilon}\int_{\{\phi=r\}} \frac{1}{\varepsilon}\zeta\left(\frac{\phi}{\varepsilon}\right) f\,d\boldsymbol{\sigma}\,dr &= \int_{|\phi(\mathbf{x})|<\varepsilon} \frac{1}{\varepsilon}\zeta\left(\frac{\phi}{\varepsilon}\right) f|\boldsymbol{\nabla}\phi|\,d\mathbf{x}\\ &= \int_{\mathbb{R}^2} \frac{1}{\varepsilon}\zeta\left(\frac{\phi}{\varepsilon}\right) f|\boldsymbol{\nabla}\phi\,|d\mathbf{x}\end{aligned}$$

Therefore,

$$\lim_{\varepsilon\to 0}\int_{\mathbb{R}^2} \frac{1}{\varepsilon}\zeta\left(\frac{\phi}{\varepsilon}\right)|\boldsymbol{\nabla}\phi| f\,d\mathbf{x} = \int_{\{\phi=0\}} f d\boldsymbol{\sigma} \quad \square$$

### 2.4. *Elastic energy and force*

In [3] we derived the elastic force from an energy of the form (2.1) written in terms of the level set function, then derived a singular force from this energy and finally regularized this force. Here we adopt the alternative and more intrinsic point of view of deriving the force directly from a regularized energy.

Let $\Omega$ be cube[a] in $\mathbb{R}^n$ which contains the fluid and membrane with, for example, periodic boundary conditions on $\mathbf{u}$ and $\phi$. We introduce

$$\mathcal{E}(\phi) = \int_\Omega E(|\boldsymbol{\nabla}\phi|)\frac{1}{\varepsilon}\zeta(\frac{\phi}{\varepsilon})d\mathbf{x}$$

where $E$ is a given constitutive law such that $E(1) = 0$. Note that $r \to E'(r)$ describes the (possibly nonlinear) stress-strain relationship.

Let $\delta : \Omega \to \mathbb{R}$ be a regular periodic test function, then the variational derivative at $\phi$ in direction $\delta$ is

$$\begin{aligned}d\mathcal{E}(\phi)(\delta) &= \int_\Omega E'(|\boldsymbol{\nabla}\phi|)\frac{\boldsymbol{\nabla}\phi\cdot\nabla\delta}{|\boldsymbol{\nabla}\phi|}\frac{1}{\varepsilon}\zeta(\frac{\phi}{\varepsilon}) + E(|\boldsymbol{\nabla}\phi|)\frac{1}{\varepsilon^2}\zeta'(\frac{\phi}{\varepsilon})\delta d\mathbf{x}\\ &= -\int_\Omega \boldsymbol{\nabla}\cdot\left[E'(|\boldsymbol{\nabla}\phi|)\frac{\boldsymbol{\nabla}\phi}{|\boldsymbol{\nabla}\phi|}\frac{1}{\varepsilon}\zeta(\frac{\phi}{\varepsilon})\right]\delta - E(|\boldsymbol{\nabla}\phi|)\frac{1}{\varepsilon^2}\zeta'(\frac{\phi}{\varepsilon})\delta d\mathbf{x}\\ &= -\int_\Omega \boldsymbol{\nabla}\cdot\left[E'(|\boldsymbol{\nabla}\phi|)\frac{\boldsymbol{\nabla}\phi}{|\boldsymbol{\nabla}\phi|}\right]\frac{1}{\varepsilon}\zeta(\frac{\phi}{\varepsilon})\delta + (E'(|\boldsymbol{\nabla}\phi|)|\boldsymbol{\nabla}\phi| - E(|\boldsymbol{\nabla}\phi|))\frac{1}{\varepsilon^2}\zeta'(\frac{\phi}{\varepsilon})\delta d\mathbf{x}\end{aligned}$$

where the boundary integrals vanish by periodicity.
The time variation of $\mathcal{E}$ is obtained by taking $\delta = -\mathbf{u}\cdot\boldsymbol{\nabla}\phi$ since from the transport equation

$$\frac{d}{dt}\mathcal{E}(\phi) = d\mathcal{E}(\phi)(\phi_t) = d\mathcal{E}(\phi)(-\mathbf{u}\cdot\boldsymbol{\nabla}\phi).$$

Thus

$$\begin{aligned}\frac{d}{dt}\mathcal{E}(\phi) = \int_\Omega \boldsymbol{\nabla}\cdot\left[E'(|\boldsymbol{\nabla}\phi|)\frac{\boldsymbol{\nabla}\phi}{|\boldsymbol{\nabla}\phi|}\right]\frac{\boldsymbol{\nabla}\phi}{|\boldsymbol{\nabla}\phi|}|\boldsymbol{\nabla}\phi|\frac{1}{\varepsilon}\zeta(\frac{\phi}{\varepsilon})\mathbf{u}\\ + (E'(|\boldsymbol{\nabla}\phi|)|\boldsymbol{\nabla}\phi| - E(|\boldsymbol{\nabla}\phi|))\frac{1}{\varepsilon^2}\zeta'(\frac{\phi}{\varepsilon})\boldsymbol{\nabla}\phi\cdot\mathbf{u}\,d\mathbf{x}.\end{aligned}$$

[a]We could make the same developments for any bounded subset of $\mathbb{R}^n$ with Dirichlet boundary conditions on $\mathbf{u}$.

Using $\boldsymbol{\nabla} \cdot \mathbf{u} = 0$ and integrating by parts the second term in the above expression leads by periodicity to:

$$\begin{aligned}\int_\Omega (E'(|\boldsymbol{\nabla}\phi|)|\boldsymbol{\nabla}\phi| - E(|\boldsymbol{\nabla}\phi|))\boldsymbol{\nabla}\left[\frac{1}{\varepsilon}\zeta(\frac{\phi}{\varepsilon})\right]\cdot \mathbf{u} d\mathbf{x} \\ = \int_\Omega (E'(|\boldsymbol{\nabla}\phi|)|\boldsymbol{\nabla}\phi| - E(|\boldsymbol{\nabla}\phi|))\boldsymbol{\nabla}\cdot\left[\frac{1}{\varepsilon}\zeta(\frac{\phi}{\varepsilon})u\right] d\mathbf{x} \\ = -\int_\Omega (\boldsymbol{\nabla}[E'(|\boldsymbol{\nabla}\phi|)]|\boldsymbol{\nabla}\phi| + E'(|\boldsymbol{\nabla}\phi|)\boldsymbol{\nabla}|\boldsymbol{\nabla}\phi| - \boldsymbol{\nabla}[E(|\boldsymbol{\nabla}\phi|)])\frac{1}{\varepsilon}\zeta(\frac{\phi}{\varepsilon})\mathbf{u} d\mathbf{x} \\ = -\int_\Omega \boldsymbol{\nabla}[E'(|\boldsymbol{\nabla}\phi|)]|\boldsymbol{\nabla}\phi|\frac{1}{\varepsilon}\zeta(\frac{\phi}{\varepsilon})\mathbf{u}\, d\mathbf{x}.\end{aligned}$$

Therefore

$$\frac{d}{dt}\mathcal{E}(\phi) = \int_\Omega \boldsymbol{\nabla}\cdot\left[E'(|\boldsymbol{\nabla}\phi|)\frac{\boldsymbol{\nabla}\phi}{|\boldsymbol{\nabla}\phi|}\right]\frac{\boldsymbol{\nabla}\phi}{|\boldsymbol{\nabla}\phi|}|\boldsymbol{\nabla}\phi|\frac{1}{\varepsilon}\zeta(\frac{\phi}{\varepsilon})\mathbf{u} - \boldsymbol{\nabla}[E'(|\boldsymbol{\nabla}\phi|)]|\boldsymbol{\nabla}\phi|\frac{1}{\varepsilon}\zeta(\frac{\phi}{\varepsilon})\mathbf{u}\, d\mathbf{x}$$

The time variation of elastic energy corresponds to the opposite of the work of the elastic force $\mathbf{F}(x,t)$. We thus have

$$\frac{d}{dt}\mathcal{E}(\phi) = -\int_\Omega \mathbf{F}(\mathbf{x},t)\cdot\mathbf{u} d\mathbf{x} \tag{2.3}$$

which gives by identification:

$$\mathbf{F}(\mathbf{x},t) = \left\{\boldsymbol{\nabla}[E'(|\boldsymbol{\nabla}\phi|)] - \boldsymbol{\nabla}\cdot\left[E'(|\boldsymbol{\nabla}\phi|)\frac{\boldsymbol{\nabla}\phi}{|\boldsymbol{\nabla}\phi|}\right]\frac{\boldsymbol{\nabla}\phi}{|\boldsymbol{\nabla}\phi|}\right\}|\boldsymbol{\nabla}\phi|\frac{1}{\varepsilon}\zeta(\frac{\phi}{\varepsilon}). \tag{2.4}$$

It maybe desirable to develop the tangential and normal components of this force. Denoting by $\mathbb{P}_{\boldsymbol{\nabla}\phi^\perp}$ the projection over the hyperplane orthogonal to $\boldsymbol{\nabla}\phi$, i.e.

$$\mathbb{P}_{\boldsymbol{\nabla}\phi^\perp}(\mathbf{v}) = \mathbf{v} - (\mathbf{v}\cdot\frac{\boldsymbol{\nabla}\phi}{|\boldsymbol{\nabla}\phi|})\frac{\boldsymbol{\nabla}\phi}{|\boldsymbol{\nabla}\phi|}$$

one can write the normal and tangential components of this elastic force:

$$F(\mathbf{x},t) = \left\{\mathbb{P}_{\boldsymbol{\nabla}\phi^\perp}(\boldsymbol{\nabla}[E'(|\boldsymbol{\nabla}\phi|)]) - E'(|\boldsymbol{\nabla}\phi|)\kappa(\phi)\frac{\boldsymbol{\nabla}\phi}{|\boldsymbol{\nabla}\phi|}\right\}|\boldsymbol{\nabla}\phi|\frac{1}{\varepsilon}\zeta(\frac{\phi}{\varepsilon}).$$

Note that, as in Peskin's Lagrangian formulation, the curvature of the membrane appears in the normal component of the force, while only variations of the stretching contribute to tangential components.

### 2.5. *Final model and conservation principles*

We first observe that the level set function also enables us to handle flows with variable density and viscosity and membranes carrying mass in a natural way. Let $H(r) = \int_{-\infty}^{r}\zeta(s)ds$, which satisfies $H(r) = 0$ for $r < -1$, and $H(r) = 1$ for $r > 1$. Let us denote by $\rho_i$ and $\rho_e$ respectively the density of the flow inside and outside the membrane, and by $\lambda_\theta$ the surface density of the membrane. If we set $\bar{\rho} = (\rho_e + \rho_i)/2$, $\delta\rho = (\rho_e - \rho_i)/2$, the density and viscosity of the whole continuous medium can be defined in a level set formulation by

$$\rho(\phi) = \bar{\rho} + H(\frac{\phi}{\varepsilon})\delta\rho + \lambda_\theta\frac{1}{\varepsilon}\zeta\left(\frac{\phi}{\varepsilon}\right)$$

where $\lambda_\theta$ is the (constant) surface density of the membrane, and

$$\mu(\phi) = \mu_1 + H(\frac{\phi}{\varepsilon})(\mu_2 - \mu_1)$$

Using (2.2), it is a simple matter to check that the above density satisfies the mass conservation equation

$$\frac{\partial\rho}{\partial t} + (\mathbf{u}\cdot\boldsymbol{\nabla})\rho = 0.$$

Conservation of momentum and volume are finally expressed by the following system

$$\begin{cases} \rho(\phi)(\mathbf{u}_t + \mathbf{u}\cdot\boldsymbol{\nabla}\mathbf{u}) - \boldsymbol{\nabla}\cdot(\mu(\phi)d(\mathbf{u})) + \boldsymbol{\nabla}p = \mathbf{F}(\mathbf{x},t), \\ \boldsymbol{\nabla}\cdot\mathbf{u} = 0, \\ \phi_t + \mathbf{u}\cdot\boldsymbol{\nabla}\phi = 0, \end{cases} \tag{2.5}$$

where $d(\mathbf{u})_{ij} = \frac{\partial u_i}{\partial x_j} + \frac{\partial u_j}{\partial x_i}$, and $F$ is defined in (2.4). These equations are complemented with periodic boundary conditions and initial conditions for $u$ and $\phi$.

To verify energy conservation, we multiply the above momentum equation by $\mathbf{u}$. Using (2.3) and integrating in space and time, we easily obtain the following conservation principle:

$$\frac{1}{2}\int_\Omega \rho(\phi)\mathbf{u}^2(x,T)\,d\mathbf{x} + \frac{1}{2}\int_0^T\int_\Omega \mu(\phi)d(\mathbf{u})^2\,d\mathbf{x}\,dt + \int_\Omega E(|\boldsymbol{\nabla}\phi|)\frac{1}{\varepsilon}\zeta(\frac{\phi}{\varepsilon})(x,T)\,d\mathbf{x} = \frac{1}{2}\int_\Omega \rho(\phi_0(x))\mathbf{u}_0^2(x)\,d\mathbf{x} + \int_\Omega E(|\boldsymbol{\nabla}\phi_0|)\frac{1}{\varepsilon}\zeta(\frac{\phi_0}{\varepsilon})\,d\mathbf{x}. \tag{2.6}$$

We recognize in this identity the conservation, up to viscous dissipation, of total -kinetic plus elastic - energy. This conservation principle is of great importance when modeling fluid-structure interaction problems.

To conclude this section, we make the following remarks. First it is important to notice that, except in the case where $\rho$ is constant (i.e. $\rho_i = \rho_e$ and $\lambda_\theta = 0$), the nonlinear terms $\mathbf{u}\cdot\boldsymbol{\nabla}\mathbf{u}$ are needed for this energy identity to hold. This is related to the already observed fact that a fluid-structure coupling with a Stokes approximation could be unstable [7]. Next, we point out that the same energy identity holds in the case of homogeneous boundary conditions on $u$ (and thus no boundary condition on $\phi$), with the assumption $|\phi| > \varepsilon$ on $\partial\Omega$ (i.e. the elastic structure does not touch the boundary).

## 3. Implementation issues and numerical illustrations

In this section we first discuss the problem of distortions in the level set function and describe a renormalization technique which avoids reinitializing the level set function at each time-step. We then shortly describe our finite-difference solver for the Navier-Stokes and advection equations. We also make a comment on the combined use of particle and level set methods.

### 3.1. *Calculation of level set forces*

In application in multi-fluids flows, level set methods are generally based on the following ingredients

- the smoothing of the singular Dirac force into a smooth function on a scale $\varepsilon \ll 1$
- the sampling of this smooth function on grid points

The first point amounts to writing

$$\delta_\Gamma(\mathbf{x}) \approx \frac{1}{\epsilon}\,|\boldsymbol{\nabla}\phi(\mathbf{x})|\,\zeta\left(\frac{\phi(\mathbf{x})}{\epsilon}\right)$$

where $\Gamma$ is the interface corresponding to the level set $\phi = 0$, $\mathbf{n}$ its normal and $\zeta$ a one dimensional smoothing function. In all our calculations we choose

$$\zeta(y) = \begin{cases} \frac{1}{2}(1+\cos\pi y) & \text{if } |y|<1 \\ 0 & \text{elsewhere.} \end{cases}$$

Assuming for simplicity a 1D interface parametrized by $\xi \to \boldsymbol{\gamma}(\xi)$, the meaning of the above approximation is that, for a given test function $\psi$ we have

$$\int_\Gamma \psi(\boldsymbol{\gamma}(\xi))|\frac{\partial\boldsymbol{\gamma}}{\partial\xi}|\,d\xi \approx \frac{1}{\epsilon}\int |\boldsymbol{\nabla}\phi(\mathbf{x})|\,\zeta\left(\frac{\phi(\mathbf{x})}{\epsilon}\right)\psi(\mathbf{x})\,d\mathbf{x}. \tag{3.1}$$

The second stage of the level set approximation consists of a quadrature of the integral in the left hand side above. The example of a plane interface, say

$$\Gamma = \{\mathbf{x}, x_2 = 0\}\ , \phi(\mathbf{x}) = \lambda x_2,$$

illustrates well the numerical errors involved in both stages of the approximation. In that case, it is easily seen that the level set method breaks down to the following approximation

$$\int \psi(x_1, 0)\, dx_1 = \frac{\lambda}{\epsilon} h^2 \sum_{i,j} \psi(ih, jh)\zeta(\frac{\lambda ih}{\epsilon}) + O\left(\frac{\lambda^2 h^2}{\epsilon^2}\right) + O\left(\frac{\epsilon^2}{\lambda^2}\right).$$

A small value for the gradient of $\phi$ at the interface ($\lambda$ in that example) thus results in a large smoothing error (the term $O\left(\frac{\epsilon^2}{\lambda^2}\right)$ in the above right hand side), while a sharp gradient increases the sampling error (the term $O\left(\frac{\lambda^2 h^2}{\epsilon^2}\right)$). A common strategy to avoid these difficulties is to enforce the gradient to take a normalized value (typically 1) at the interface through a reinitialization step which consists of solving the PDE

$$\frac{\partial \phi}{\partial \tau} + \mathrm{sgn}(\phi_0)(|\boldsymbol{\nabla}\phi| - 1) = 0. \tag{3.2}$$

This method has several drawbacks: firstly it involves some additional work; the desired value of the level set function is obtained as the asymptotics $\tau \to +\infty$ for (3.2). In practice a rule of thumb is that it requires a number of time steps of the order of the number of grid-points in the support of the smoothing function. The second difficulty associated with reinitialization is the numerical discrepancy in the location of the interface that can result from solving (3.2). This difficulty is recognized in [6]. In this paper the authors observed that for low resolution calculation in a strongly sheared flow solving equation (3.2) can result in a complete loss of the interface. They proposed a correction method based on a particle scheme to restore the proper location of the interface (we will comment later more specifically on this algorithm).

Finally in our case, where the level set function is associated to the stretching of the immersed boundaries, solving (3.2) at every time step would require to monitor and reset to the correct value the stretching of the interface. This would add some complexity to the method that we wanted to avoid.

To overcome these difficulties we have observed that it is possible to use the original level set function, that is the solution to (2.2), provided it is properly renormalized in the expression of the mollified forces. In other words the expression

$$\frac{1}{\epsilon} |\boldsymbol{\nabla}\phi(\mathbf{x})|\ \zeta\left(\frac{\phi(\mathbf{x})}{\epsilon}\right) \tag{3.3}$$

has to be replaced everywhere by

$$\frac{1}{\epsilon}\, \zeta\left(\frac{\phi(\mathbf{x})}{\epsilon|\boldsymbol{\nabla}\phi(\mathbf{x})|}\right) \tag{3.4}$$

A Taylor expansion easily reveals that the effect of this normalization is to maintain the effective spreading of the interface at a constant value, of the order of $\varepsilon$, at any time. This method was combined in [2] with a particle method for the numerical simulation of variable-density flows with surface tension. In the sequel we will show numerical validations of this technique for the transport of the interface in flows with large deformations. For this we will compare the reinitialization by (3.2) with our renormalisation procedure. For these tests, equation (3.2) was solved using a fifth order WENO scheme, with the following explicit Godunov flux [9]

$$H_{ij}(u^+, u^-, v^+, v^-) = \begin{cases} s_{ij}(\sqrt{[\max([u^+]_-, [u^-]_+)]^2 + [\max([v^+]_-, [v^-]_+)]^2} - 1) & \text{if } s_{ij} > 0, \\ s_{ij}(\sqrt{[\max([u^+]_+, [u^-]_-)]^2 + [\max([v^+]_+, [v^-]_+)]^2} - 1) & \text{else,} \end{cases}$$

with the approximate sign function

$$s_{ij} = \frac{\phi^0_{ij}}{\sqrt{{\phi^0_{ij}}^2 + dx}}$$

and using a third order Runge-Kutta method for the pseudo-time iteration.

### 3.2. *Navier-Stokes solver and advection equation*

Our numerical discretization uses a staggered grid upon which we compute at discrete times $t_n$ the quantities $\phi^n$, $p^n$ and $\mathbf{u}^n$. The level set function and the pressure are defined on grid points, whereas the horizontal (resp. vertical) velocity is defined on the vertical (resp. horizontal) edges (MAC method). The Navier-Stokes equations are solved using Chorin's projection method, in its explicit or Crank-Nicolson form [10]. One time iteration of our algorithm proceeds as follows:

- Compute the tentative velocity field of the projection method by solving the momentum equation without the pressure term. The nonlinear advection terms are explicitly computed by a fifth order WENO scheme [17]. The viscous terms are dicretized by a central scheme. In the case of variable viscosity, we discretize the following form of the viscous term:

$$\boldsymbol{\nabla}\cdot(\mu(\phi)d(\mathbf{u})) = \begin{pmatrix} 2\frac{\partial}{\partial x}\left[\mu(\frac{\phi}{\varepsilon|\boldsymbol{\nabla}\phi|})\frac{\partial u}{\partial x}\right] + \frac{\partial}{\partial y}\left[\mu(\frac{\phi}{\varepsilon|\boldsymbol{\nabla}\phi|})(\frac{\partial u}{\partial y}+\frac{\partial v}{\partial x})\right] \\ 2\frac{\partial}{\partial y}\left[\mu(\frac{\phi}{\varepsilon|\boldsymbol{\nabla}\phi|})\frac{\partial v}{\partial y}\right] + \frac{\partial}{\partial x}\left[\mu(\frac{\phi}{\varepsilon|\boldsymbol{\nabla}\phi|})(\frac{\partial u}{\partial y}+\frac{\partial v}{\partial x})\right] \end{pmatrix}.$$

  The elastic force is computed by a straightforward centered discretization of (2.4), for those points $(i,j)$ which are close enough to the interface so that

$$\frac{|\phi_{ij}|}{|\boldsymbol{\nabla}\phi|_{ij}} < \varepsilon.$$

- Solve for the pressure using a Poisson solver based on classical 5 (in 2D) or 7 points (in 3D) second order stencils.
- Solve the transport equation (2.2) still using the fifth order WENO scheme.

All numerical results presented thereafter have been obtained with an explicit Euler time discretisation, with a time step corresponding to a CFL number of $0.1$, which turned to be sufficient, for the low Reynolds considered in that paper, to ensure stability of the coupling. However a precise stability analysis of the fluid-structure coupling remains to be done and will be adressed in a future work. More extensive three dimensional simulations will clearly require more appropriate schemes.

## 4. Numerical results

### 4.1. *Renormalization vs reinitialization of the level set function*

In this section we compare (3.2) and (3.4). In a level set method one has to be concerned with two issues: compute the correct location of the interface and the correct forces on the interface. The latter is clearly conditioned by the former and by the control of truncation errors in the mollification and sampling of the forces as discussed above.

Surprisingly however it seems that, unlike the interface location which is associated to volume conservation, the force calculation is seldom looked at in validation studies of level set methods. In the numerical illustrations that follow we have focused on a passive interface in a complex flow and we have monitored both the interface location and its length, as an example of diagnostic of interface forces obtained with the test-function value $\psi \equiv 1$ in (3.1). With the original formula (3.3) we obtain the following definition of the length

$$\mathcal{L}_1(\Gamma) = \frac{1}{\epsilon}\int |\boldsymbol{\nabla}\phi(\mathbf{x})|\,\zeta\left(\frac{\phi(\mathbf{x})}{\epsilon}\right)\,d\mathbf{x} \tag{4.1}$$

and, with the normalization (3.4):

$$\mathcal{L}_2(\Gamma) = \frac{1}{\epsilon}\int \zeta\left(\frac{\phi(\mathbf{x})}{\epsilon|\boldsymbol{\nabla}\phi(\mathbf{x})|}\right)\,d\mathbf{x} \tag{4.2}$$

The example we consider below is borrowed from [6]. It consists of the passive transport of a circle in a flow created by a vortex (see figure 1). This flow develops high strain which results in the creation of filaments on the interface which spirals around the origin.

In figure 2 we compare the length of the interface computed by formulas (4.1,4.2) with a reference value for different resolutions. The reference value is obtained by explicitly tracking a large number of markers on the interface. One observes that, as time goes on, the low resolution calculations are not able to capture the complete spiral of the interface. For a $128 \times 128$ calculation, formula (4.1) where the level set function has been restarted with (3.2) at every time step, leads to a complete loss of the interface after $t = 5$. This confirms the observation made in [6]. By contrast the normalized formula (4.2) is able to retain at least part of the interface. Note however that in an intermediate time range, the reinitialization method seems to work better that the normalized method, for all grid-sizes, and that for medium to high resolution reinitiliazation provides slightly better interface location. The reason is probably that, by enforcing normalized values of the gradient of the level set function, this method tends to reduce the truncation error in the discretization for the advection equation (see below for results when renormalization is coupled with particle methods). This advantage would however disappear when the flow itself has sharp discontinuities at the interface, which is the case of the flow-structure interaction problem we are interested in.

In figure 3 we show the interface computed on $256 \times 256$ and $512 \times 512$ grids by both the renitialized or normalized formulas and reference front tracking solution.

A first conclusion of these calculations is that the renormalization technique (3.4) provides an economical and efficient alternative of the classical reinitialization techniques.

To finish with this section we wish to make a comment on the use of particle methods in conjonction with level set methods (see also [8]). In [6] a correction method to remedy the discrepancy in the interface tracking for low resolution reinitialized level set method was proposed based on the use of Lagrangian markers near the interface. As a matter of fact, it is well-known since the computations of Anderson and Krasny in the early 80's, that particle methods are well-adapted for interface capturing. In the framework of level set methods, if a discretization of the gradient of the level set function is used, particles automatically adjust to the neighborhood of the interface [2]. In the example showed in figure 4 we have used a plain particle method with a grid size of $h = 1/512$. The initial level set function is a gaussian profile spreading on 2 particles on each directions. The renormalized method (3.4) was used to compute interface length. In [6] the authors use 4 Lagrangian markers per grid-size along each direction to correct a Weno discretization of the pure level set method with $128 \times 128$ grid points to correct a Weno discretization of the pure level set method with $128 \times 128$ grid points. The numbers of particles should therefore roughly correspond. By plain particle method we mean a particle method where particles are pushed and their strength updated through the solution of a system of ODE's, in our case discretized by classical second order Runge Kutta, and remeshed at every time-step through interpolation with a kernel preserving third order accuracy. In figure 4 we have plotted the lengths obtained by the particle method compared to the reference front-tracking solution and the $512 \times 512$ WENO solution.

Finally, we have also performed the time-reversed calculation suggested in [6]: the velocity is modulated at time $t$ by a factor $cos(\pi t/8)$ which should have the effect of recalling the interface back to its original state at time $t = 8$. For that experiment the number of particles ranges from $6000$ at time $0$ to about $80000$ at time $8$ (the actual number of particles used in [6] is not mentioned by the authors). The initial volume is conserved up to a relative error of about $10^{-4}$, to be compared to the values $0.0071$ and $0.0035$ reported in [6] for their particle level set method based on grids with $128$ and $256$ grid points in each direction (this would correspond to inter-particle spacing $h = 1/512$ and $h = 1/1024$ in our implementation). The length of the interface, computed by the normalized formula (4.2) is computed with an accuracy of $0.2\%$. Figure 5 we show the interface obtained at time $8$ compared to the exact circular shape. Although the interface obtained in [6] is in a slightly better agreement with the exact solution, the genuine particle level set algorithm, given its simplicity, appears a rather efficient tool to capture complex interfaces.

### 4.2. *Validation case for the fluid-structure model: pressurized membranes*

We now turn to the validation study of the level set method (2.5). We focus on a two-dimensional test case studied in [11] and then turn to its three-dimensional extension. Following [11] we consider the case of a pressurized membrane, with the same parameters. Starting from a circular membrane, we stretch it into an ellipse. To balance the stretching force the flow develops a sharp pressure gradient at the interface. The membrane, to reach its minimal elastic energy, relaxes to a circular shape that preserves the initial volume. The time-scale on which this equilibrium is reached depends on the viscous dissipation acting on the flow.

The parameters are the same as in [11]: the unstretched circle has a radius 0.5 in a computation box of size $2 \times 2$. The initial membrane is an ellipse of major and minor axes $a = 0.75, b = 0.5$. This gives a length of $3.96636$ and therefore a stretching factor of about $1.262$. The equilibrium circle has a radius $r = \sqrt{ab} \simeq 0.61237$. The numerical method for this test is the finite difference method described in section 3.2. The viscosity coefficient is $0.01$. The boundary conditions enforce zero velocity at the boundary of the box. Although in principle the ratio $h/\varepsilon$ should tend to 0 as the grid is refined we kept it equal to 2 in these calculations.

In figure 6 we show the pressure gradients at times $0.2$ and $2.2$ for $N = 64$ and $N = 256$ grid points in each direction. One can see that the pressure fronts extend to 2 grid-points. In figure 7 we have monitored the evolution of the maximum extent of the membrane along the axis. This evolution towards the equilibrium circle does not show the drift that is typical of leaking problems in classical implementations of Immersed Boundary Methods. Our results agree very well with those obtained with the Immersed Interface Method proposed in [11]. Finally figure 8 shows a refinement study for the conservation of volume monitored at time $t = 1$. In this figure we compare our results to the results reported in [11] for the original Immersed Boundary method of Peskin and the Immersed Interface method designed in this paper. Even at low resolution, the level set method behaves very well for this diagnostic. This reflects the fact that conservation is built-in the level set formulation (2.5) at the continuous level, and that using a high order scheme for the advection of the level set function maintains good conservation properties at the discrete level.

To illustrate the fact that our method easily handles more complex incompressible flows, we considered also the case of a variable viscosity. The viscosity was divided by a factor ten outside the membrane. Figure 9 shows the evolution of the radius in the $x$ and $y$ directions, while in Figure 10 the vorticity plot at time $t = 7$ is displayed. The lower viscosity leads to a significantly slower dissipation towards the equilibrium. Exchanging the viscosity values outside and inside the membrane does not lead to such a difference in the time-scales (result not shown), which indicates that the flow develops mostly outside the membrane.

Our last experiments focus on the three-dimensional case. We have considered a pressurized membrane with radius values of $0.1$, $0.3$ and $0.4$ respectively in $x$, $y$, and $z$ directions. As in the two-dimensional case, the ellipse returns to a spherical equilibrium but in a more complex dynamics, since it can expend in three different directions. A stretching factor 2 was selected for this case. This value, higher than in the two-dimensional case, was chosen to ensure that the spherical equilibrium state would maintain a higher pressure outside than inside the membrane. The Reynolds number was $100$ and we used $128$ grid points in each directions. In that case, periodic boundary conditions were implemented.

To illustrate the flow resulting from this interaction, we show in figure 11 isosurfaces of vorticity magnitude corresponding to a value of $20$ at the early stage of the dynamics ($t = 0.1$), together with pressure contours in slices of the membrane cut through the origin parallel to two different planes.

Figure 12 finally shows snapshots of the membrane location, colored by the magnitude of the stretching, and pressure fields in two meridian planes at four different times: $t = 0.3, 0.5, 0.8, 1.$. The relative error in volume conservation at that final time was about $1\%$. Although this is clearly a much higher error level than for the two dimensional case, given the complexity of the flow and the important value of the initial stretching we found it satisfactory. These plots only serve as qualitative illustrations of the method and more systematic studies are under way for larger Reynolds numbers.

## 5. Conclusion

We have presented a level set method to handle fluid-structure interaction problems when the flows are incompressible and the structures consist of immersed membranes. The method is based on the observation that the level set function carries information about surface stretching. It enjoys natural mass and energy conservation properties at the continuous level, which are also satisfied at the discrete level provided accurate finite-difference discretizations are used for the Navier-Stokes and level set function advection equations. Reinitialization techniques that are in general used in level set methods are replaced by appropriate renormalization to enable economical implementation of the method.

The method was validated in dimension two on test cases consisting of pressurized membranes. Three-dimensional experiments also demonstrate the validity of the concept in that case. Ongoing three-dimensional extension and applications of the method will allow to have a more quantitative evaluation of its capabilities. These extensions concern the implementation of bending terms in the energy potential. These terms only involve curvature and derivatives of the curvature and therefore can be conveniently handled in our level set framework. The study in particular of flow dynamics in collapsible tubes seem to be an appealing field of application of the method.

## 6. Appendix

In this section we prove the following result that has been used in the proof of Propositions 2.1 and 2.2: under assumption $(A)$, for $f$ continuous with compact support,

$$r \to \int_{\{\phi=r\}} f d\sigma$$

is continuous. The solution of (2.2) is given by $\phi(x,t) = \phi_0(X(0;x,t))$ thus

$$\nabla\phi = \nabla\phi_0(X(0;x,t))\nabla X(0;x,t).$$

As $\det \nabla X(0;x,t) = 1$ and $|\nabla\phi_0| \geq \alpha > 0$, we have $\nabla\phi \neq 0$ on $\overline{\Omega} \times [0,T]$. Moreover $\nabla\phi$ is regular and $\overline{\Omega} \times [0,T]$ compact we thus have $|\nabla\phi| \geq \beta > 0$. For the sake of simplicity here we drop the variable $t$ which is kept fixed in $[0,T]$. Thanks to assumptions $(A)$ it is straightforward to check that $\phi$ remains $\mathcal{C}^2$ for all time. As $|\nabla\phi|$ is bounded by below by a positive constant, the vector field defined by

$$w(x) = \frac{\nabla\phi}{|\nabla\phi|^2}$$

is of class $\mathcal{C}^1$. Therefore the differential system

$$\begin{cases} \frac{d}{dr}Y(r;x) = w(Y(r;x)) \\ Y(0;x) = x \end{cases}$$

has a local solution $r \to Y(r;x)$ which is $\mathcal{C}^1$ with respect to $r$ and $x$. Differentiating $r \to \phi(Y(r;x))$ immediately shows that $\phi(Y(r;x)) = \phi(x) + r$. With this construction one has $Y(r, \{\phi = 0\}) = \{\phi = r\}$.

Finally let $s \in [0,1] \to \gamma(s)$ a $\mathcal{C}^1$ parametrization of $\{\phi = 0\}$, then $s \in [0,1] \to Y(r;\gamma(s))$ is a $\mathcal{C}^1$ parametrization of $\{\phi = r\}$. Thus for any continuous $f$ with compact support,

$$r \to \int_{\{\phi=r\}} f d\sigma = \int_0^1 f(Y(r;\gamma(s)))|\nabla Y(r;\gamma(s))\gamma_s(s)|ds$$

is continous.

## References

1. Y.C. Chang, T.Y. Hou, B. Merriman, S. Osher, *A Level Set Formulation of Eulerian Interface Capturing Methods for Incompressible Fluid Flows*, J. Comp. Phys., 124, 449–464 (1996).

2. G.-H. Cottet, *Multi-physics and particle methods*, in Computational Fluid and Solid Mechanics 2003, K.J. Bathe (ed.), Elsevier (2003)
3. G.-H. Cottet et E. Maitre, *A level set formulation of immersed boundary methods for fluid-structure interaction problems*, C. R. Acad. Sci. Paris, Ser. I 338, 581-586 (2004).
4. J. Donea, S. Giuliani, and J. P. Halleux, *An arbitrary, Lagrangian-Eulerian finite element method for transient dynamic fluid-structure interactions*, Comput. Methods Appl. Mech. Eng. 33, 689 (1982)
5. L.C. Evans and R. Gariepy, *Measure theory and fine properties of functions*, CRC Press (1992).
6. D. Enright, R. Fedkiw, J. Ferziger and I. Mitchell, *A Hybrid Particle level set Method for Improved Interface Capturing*, J. Comput. Phys., 183, 83-116 (2002).
7. C. Grandmont and Y. Maday, *Existence for an unsteady fluid–structure interaction problem*, M2AN, 34 , 609–636 (2000).
8. S. Hieber and P. Koumoutsakos, *A Lagrangian particle level set method*, submitted.
9. G. Jiang and D. Peng, *Weighted ENO schemes for Hamilton–Jacobi equations*, SIAM J. Sci. Comput., 21, 2126 (2000)
10. J. Kim and P. Moin, *Application of a fractional-step method to solve incompressible Navier-Stokes equations*, J. Comput. Phys., 59 323–360 (1985)
11. L. Lee and R.J. LeVeque, *An immersed interface method for incompressible Navier-Stokes equations*, SIAM J. Sci. Comp., 25, 832–856 (2003)
12. R. J. LeVeque and Z. Li, *Immersed interface methods for Stokes flow with elastic boundaries or surface tension*, SIAM J. Sci. Comput., 18, No. 3, 709–735 (1997).
13. S. Osher and R. Fedkiw, *Level Set Methods and Dynamic Implicit Surfaces*, Springer-Verlag, New York (2002).
14. C.S. Peskin, *Numerical Analysis of Blood Flow in the Heart*, J. Comp. Phys., 25, 220–252 (1977).
15. C.S. Peskin, *The immersed boundary method* Acta Numerica, 11, 479–517 (2002).
16. S. Peskin and B.F. Printz, *Improved volume conservation in the computation of flows with immersed boundaries*, J. Comput. Phys., 105, 33–46 (1993)
17. C.-W. Shu, *Essentially non-oscillatory and weighted essentially non-oscillatory schemes for hyperbolic conservation laws*, ICASE Report No. 97-65 (techreports.larc.nasa.gov/icase/1997/icase-1997-65.pdf)
18. P. Le Tallec and J. Mouro, *Fluid structure interaction with large structural displacements*, Compt. Meth. Appl. Mech. Engrg., 190, 3039–3067 (2001)
19. C. Tu and C.S. Peskin, *Stability and instability in the computation of flows with moving immersed boundaries: A comparison of three methods*, SIAM J. Sci. Statist. Comput., 13,1361–1376 (1992).

## 7. List of figures

Figure 1: Test case of a circular interface in a vortical flow. Stationary velocity field and initial level-set function.

Figure 2: Interface lengths for the flow of figure 1 and various resolutions. Solid lines (resp. dashed lines) are for the normalized formula (4.2) (resp. formulas (3.2),(4.1)). Black curve is the reference solution. Green, red and blue curves respectively correspond to $N = 128, 256, 512$ grid points in each direction.

Figure 3: Interface location at $t = 5$ for $512 \times 512$ (top row) and $256 \times 256$ (bottom row) grid resolution for the reinitialized (left pictures) and renormalized (right pictures) level-set methods.

Figure 4: Length of the interface by a particle method with $h = 1/512$ (red curve) compared to a WENO method with a $512 \times 512$ grid (green curve) and the reference solution (black curve).

Figure 5: One period of the evolution of the interface: solution obtained by the particle method with $h = 1/512$ (red curve) compared to the exact solution (black curve).

Figure 6: Elastic membrane in a two-dimensional flow: pressure profiles for $t = 0.2$ (left picture) and $t = 2.2$ along the $x$-axis. Markers and dotted lines are respectively for $N = 64$ and $N = 256$ points in each direction.

Figure 7: Elastic membrane in a two-dimensional flow: time-evolution of ellipse radii along $x$ (dotted line) and $y$ (solid line) directions for $Re = 100$.

Figure 8: Elastic membrane in a two-dimensional flow: refinement study of the relative error in volume conservation at time $t = 1$, for $N = 64, 128$ and $256$. Dotted line: classical Immersed Boundary Method;

dashed line: Immersed Interface Method [11]; solid line: present method.

Figure 9: Elastic membrane in a two-dimensional flow: same as figure 7 with Reynolds number $1000$ outside the membrane.

Figure 10: Elastic membrane in a two-dimensional flow with Reynolds number $1000$ outside the membrane, vorticity iso-surface at time $t = 7$.

Figure 11: Elastic membrane in a three-dimensional flow: vorticity iso-surface and pressure contours in two meridian planes through center of the membrane.

Figure 12: Elastic membrane in a three-dimensional flow: membrane locations, colored by stretching magnitude, and pressure fields for times $0.3, 0.5, 0.8$ and $1$ (from left to right, top to bottom)

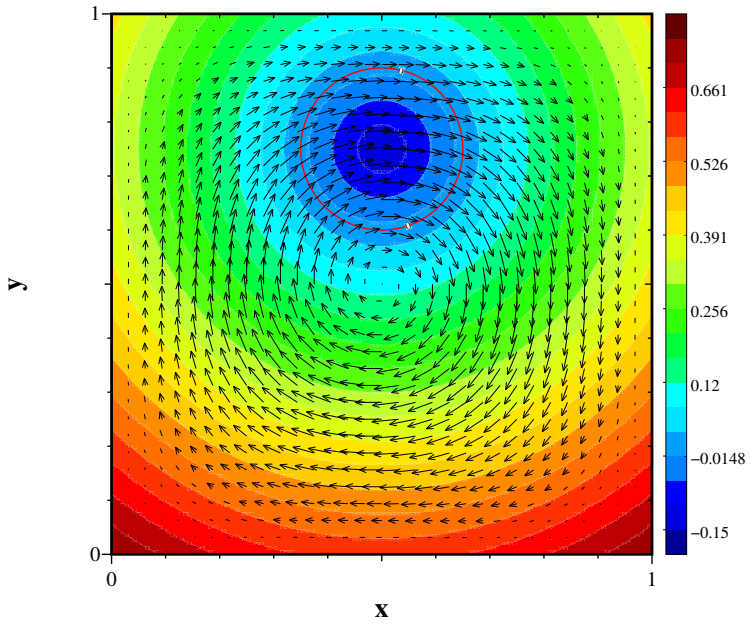


FIGURE 1.

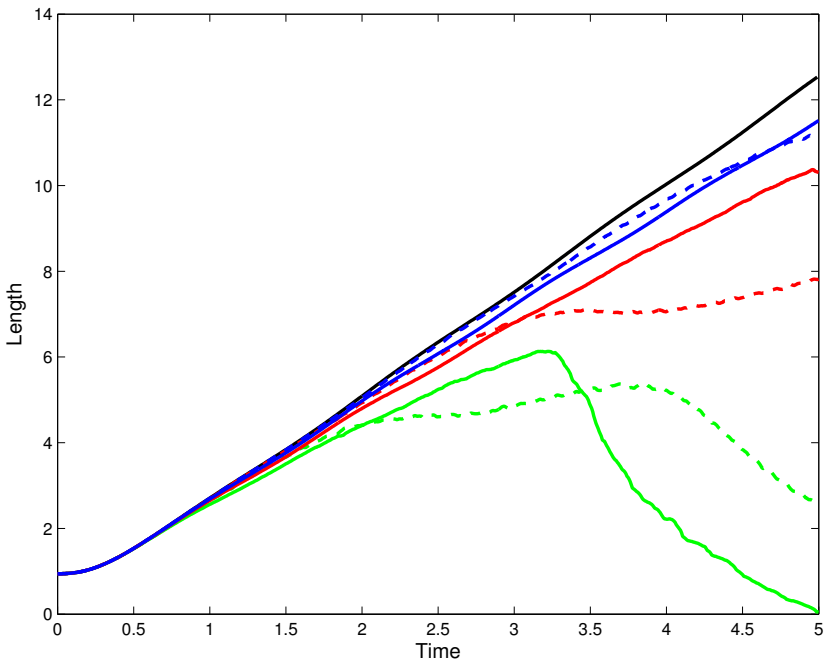


FIGURE 2.

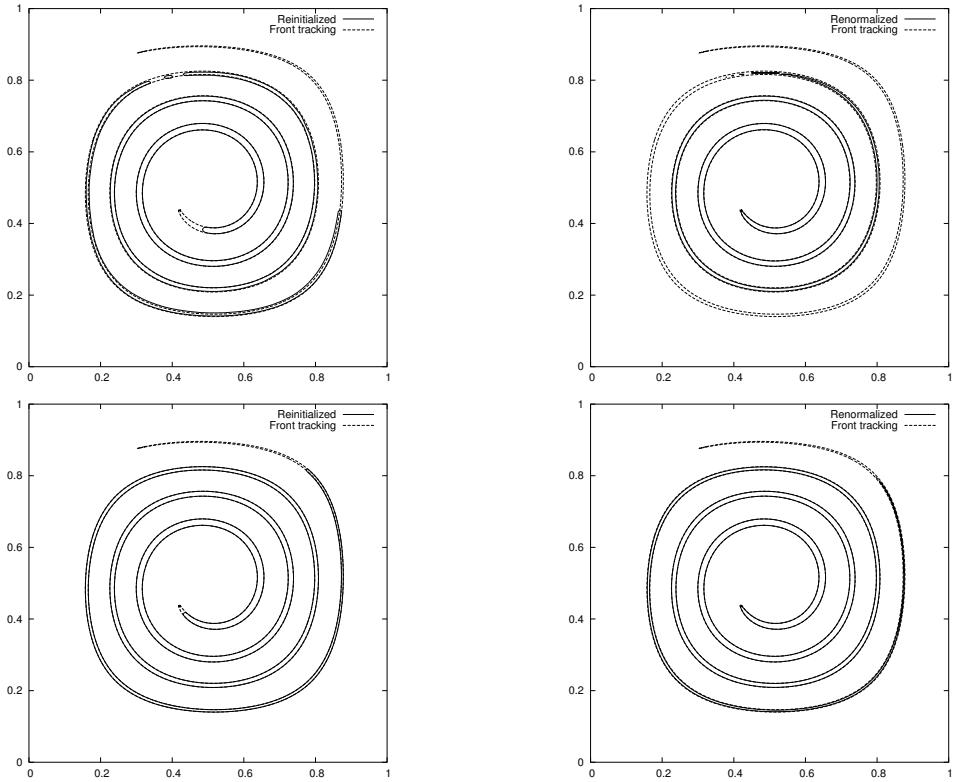


FIGURE 3.

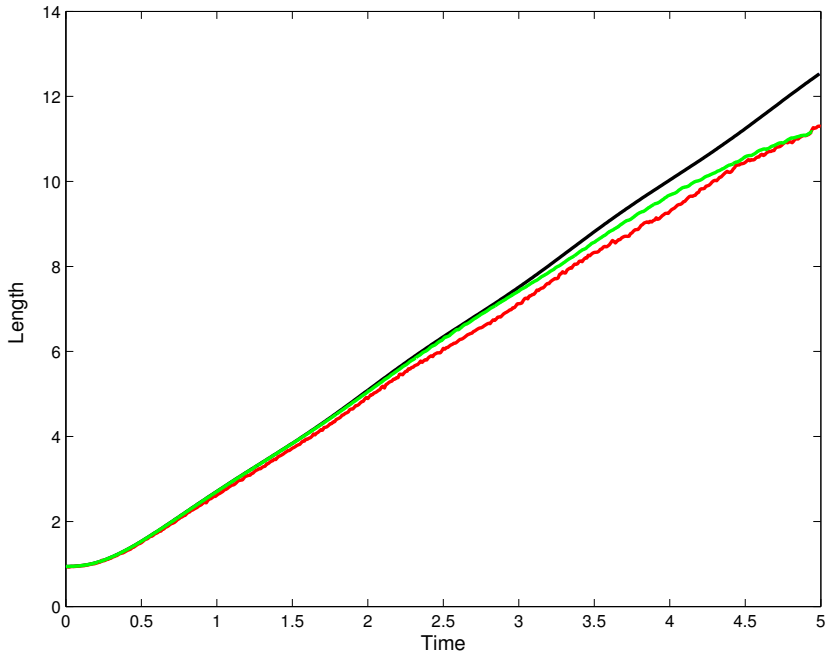


FIGURE 4.

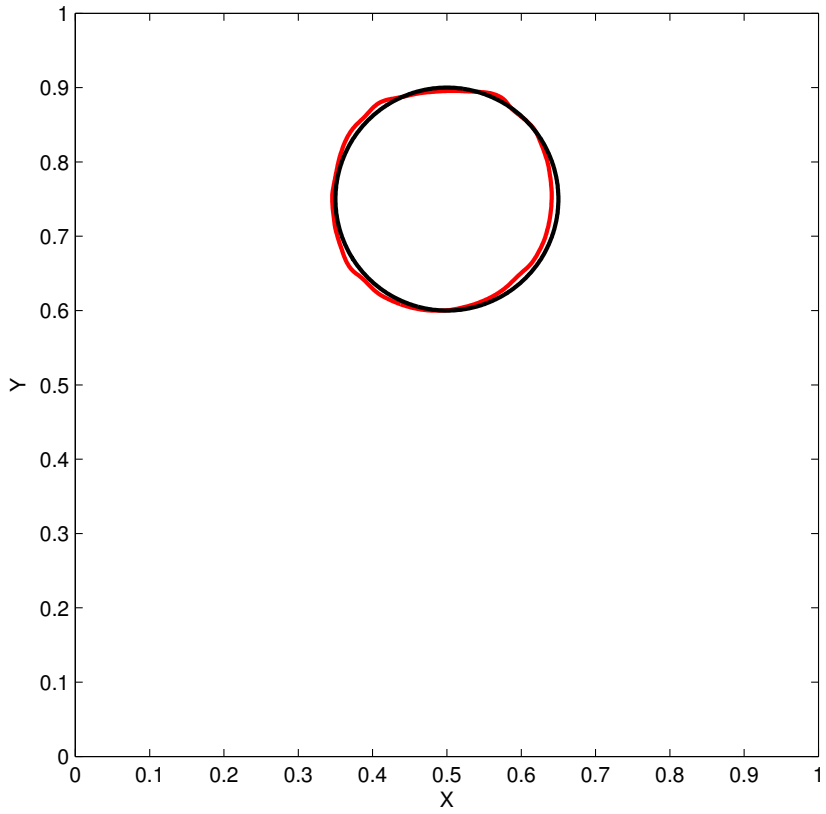


FIGURE 5.

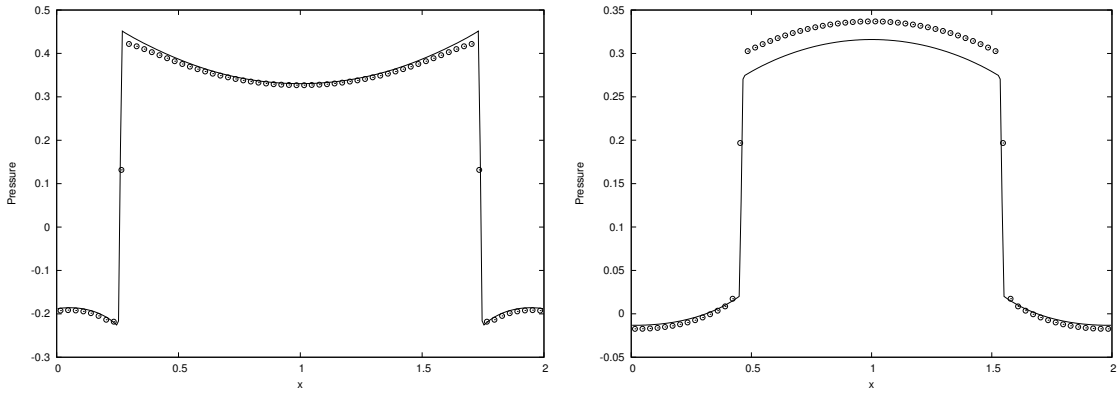


FIGURE 6.

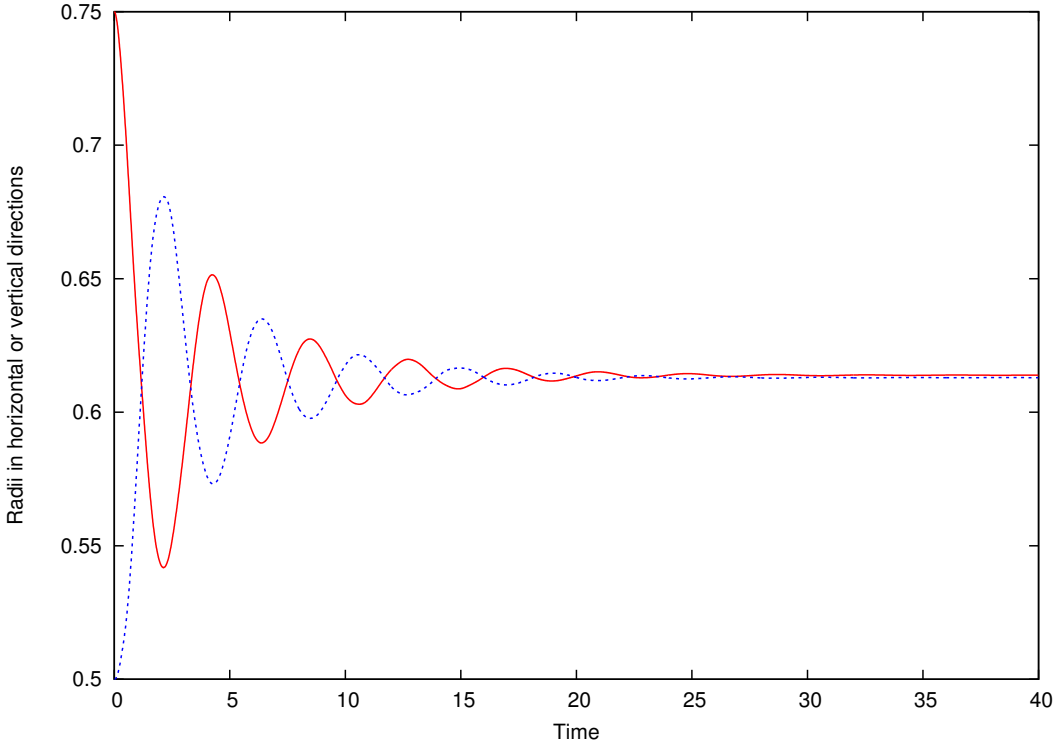


FIGURE 7.

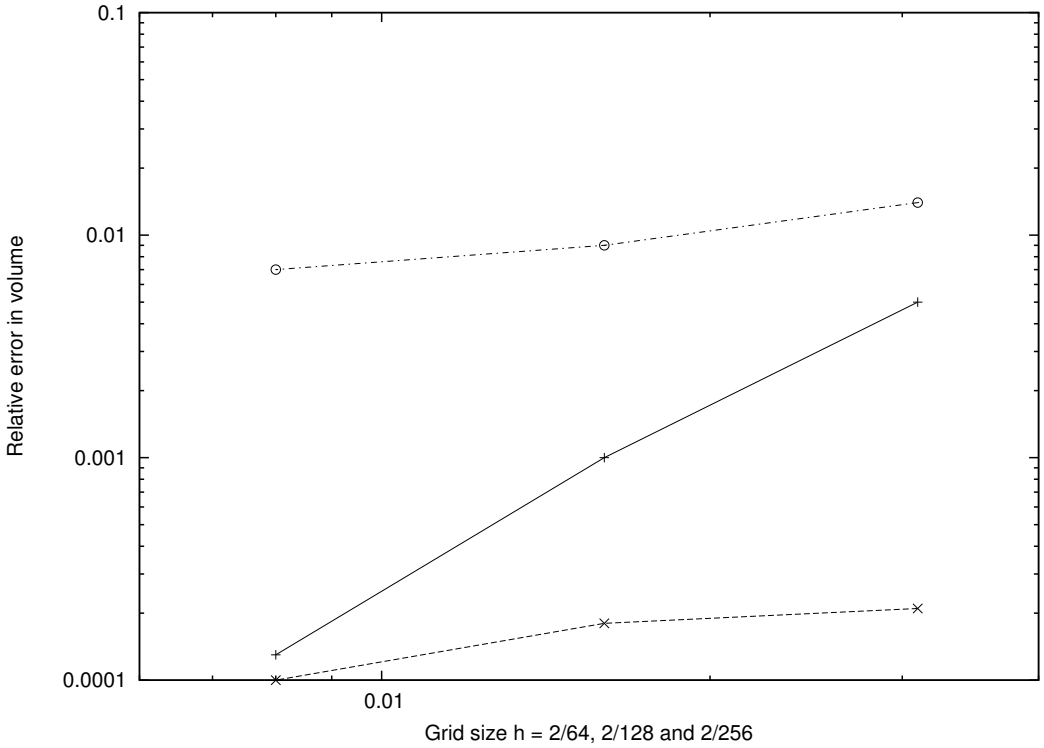


FIGURE 8.

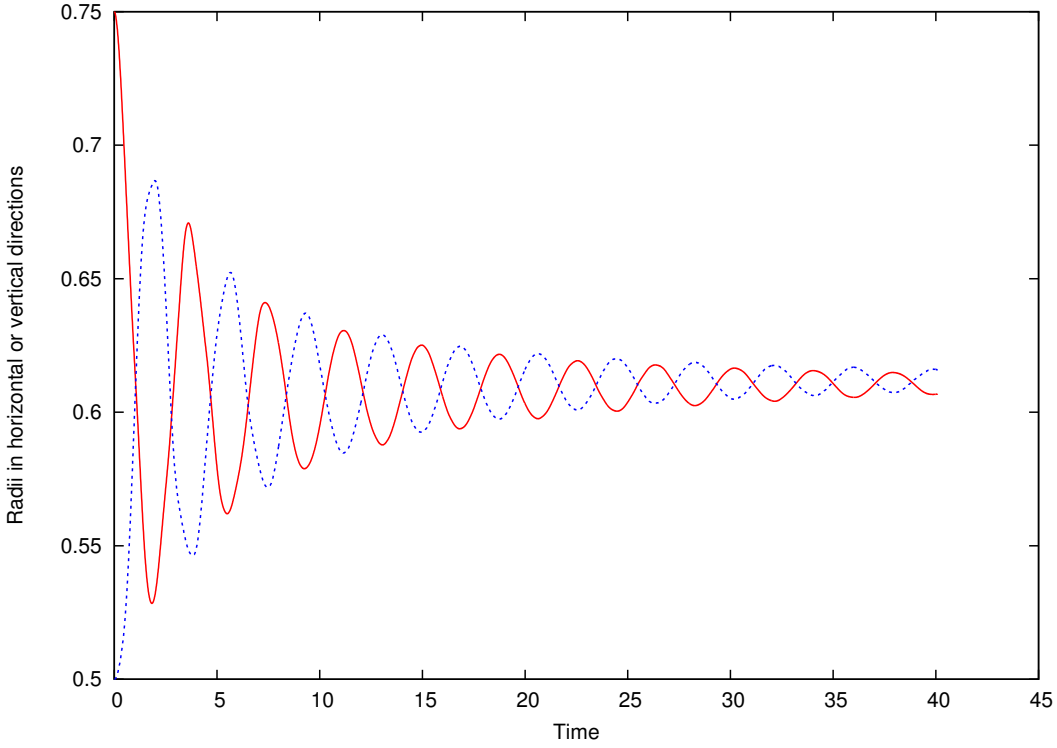


FIGURE 9.

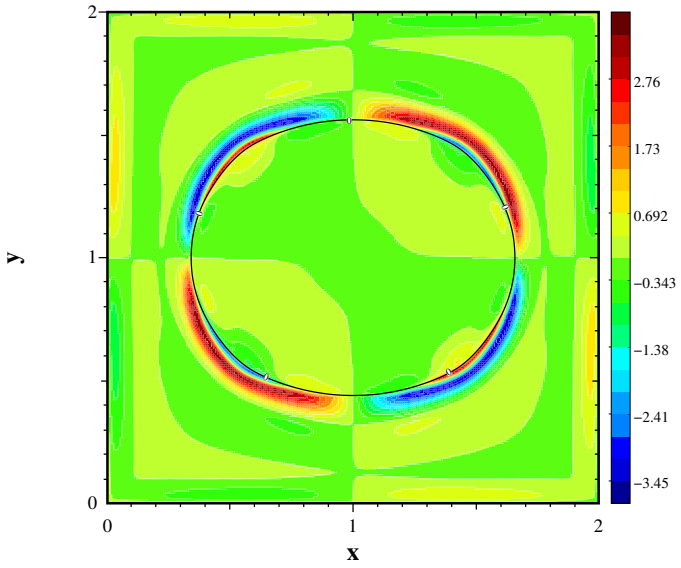


FIGURE 10.

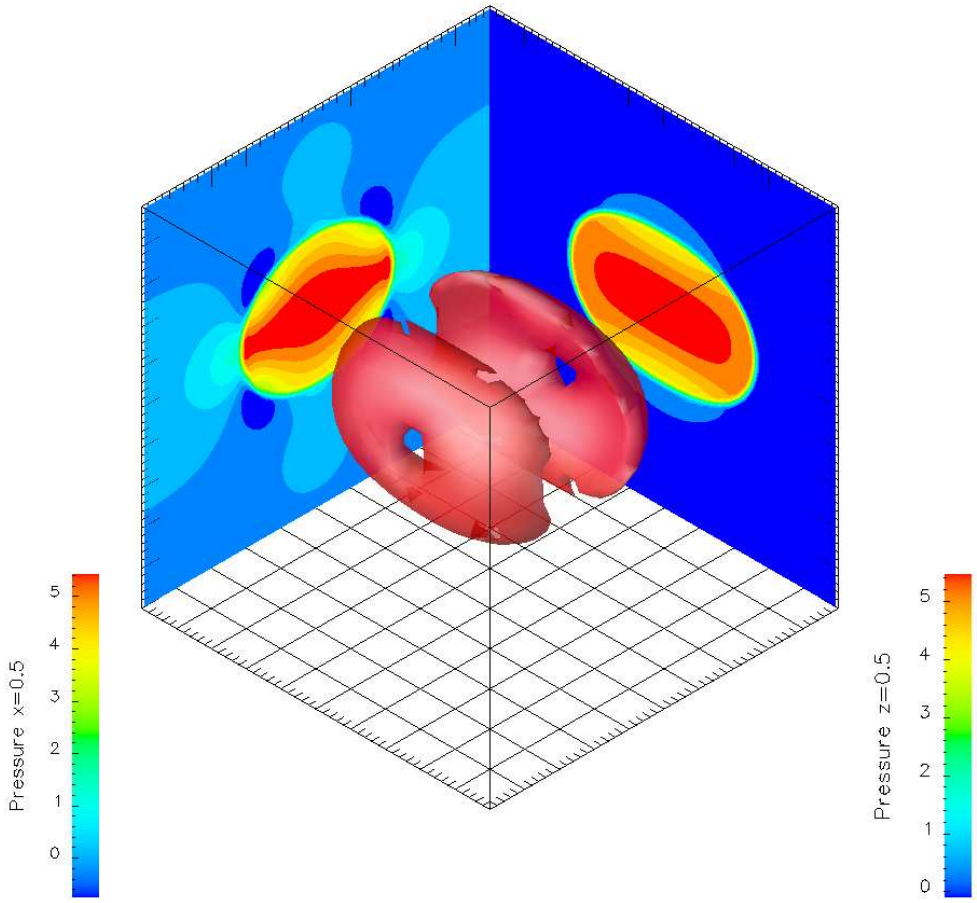


FIGURE 11.

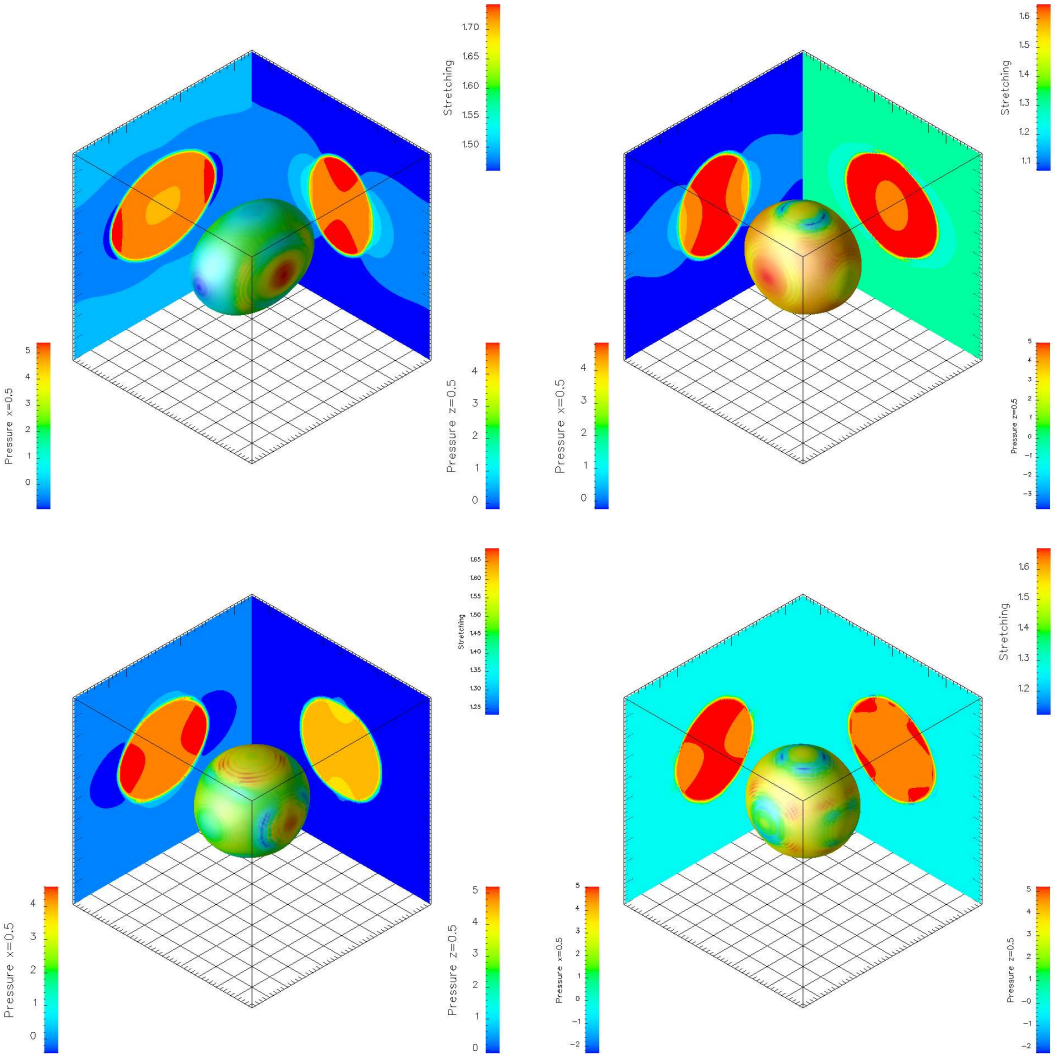


FIGURE 12.